Theoretical study of electrical conduction through a molecule connected to metallic nanocontacts

Eldon G. Emberly[*] and George Kirczenow

Department of Physics, Simon Fraser University, Burnaby, British Columbia, Canada V5A 1S6

(Received 11 May 1998)

We present a theoretical study of electron transport through a molecule connected to two metallic nanocontacts. The system investigated is 1,4 benzene-dithiolate, chemically bonded to two Au contacts. The surface chemistry is modeled by representing the tips of the Au contacts as two atomic clusters and treating the molecule-cluster complex as a single entity in an extended Hückel tight-binding scheme. We model the tips using several different cluster geometries. An ideal lead is attached to each cluster, and the lead-to-lead transmission is calculated. The role of the molecule-cluster interaction in transport is analyzed by using single-channel leads. We then extend the calculations to multichannel leads that are a more realistic model of the tip's environment. Using the finite-voltage, finite-temperature Landauer formula, we calculate the differential conductance for the different systems studied. The similarities and differences between the predictions of the present class of models and recent experimental work are discussed. [S0163-1829(98)06039-1]

I. INTRODUCTION

A molecular wire in its simplest definition consists of a molecule connected between two reservoirs of electrons. Such a system poses many interesting theoretical and experimental challenges. It was first suggested in the early 1970s by Aviram and Ratner that such a system should have the ability to rectify current.[1] Recent experiments on molecular wires have included studies of conduction in molecular thin films,[2,3] in self-assembled monolayers (SAM's) using a scanning tunnel microscope (STM),[4–8] and through a single molecule connected between the tips of a mechanically controlled break junction.[9] Theoretical work on electronic transport in these mesoscopic systems has also appeared recently.[10–14,8]

The theoretical analysis of conduction through a molecule bonded to metallic contacts brings together different methods from chemistry and physics. The treatment of the molecule itself is a problem in quantum chemistry. Many different techniques exist for the calculation of the electronic structure of molecular systems. There is also the matter of how to treat the interaction between the molecule and the surface of the metallic reservoir. This can be done using an effective interaction via Newns-Anderson[15] or by modeling the tips atomistically.[16] Once these issues have been addressed it is possible to proceed to the electron transport problem. For molecular wires with nanometer dimensions, Landauer theory[17,18] is used, which relates the conductance to the electron transmission probability.

A molecule of current experimental interest as a molecular wire,[9] and the one studied theoretically in this paper, is 1,4 benzene-dithiol, which when attached to two gold leads becomes 1,4 benzene-dithiolate (BDT). It consists of a benzene molecule with two sulfur atoms attached, one on either end of the benzene ring. The benzene offers delocalized electrons in the form of π orbitals, conducive to electron transport. The sulfurs bond effectively to the gold nanocontacts. Two major unknowns of the experimental system[9] are the geometry of the gold contacts and the nature of the bond between the molecule and these contacts. This paper attempts to address these important issues.

In our model of the BDT wire we attach the molecule to two gold clusters. Thus we consider the interactions between the molecule and tip surface at an atomistic level. This system of clusters+molecule (CMC) is then treated as a single larger molecule which we model using the extended Hückel tight-binding method of quantum chemistry. This allows us to address the chemical nature of the interface between the nanocontacts and molecule by treating the clusters and BDT as an integral entity. In this paper we consider gold clusters oriented in the (100) and (111) directions. We also examine different binding schemes for the thiol end groups of the BDT to these clusters.

Using Landauer theory and the above tight-binding model of the contact region, we proceed to study electronic transport through the system by attaching ideal leads to the backs of the clusters. We consider two types of leads in this paper. The first is a one-dimensional (1D) lead consisting of a chain of atoms with just one conducting electronic mode or channel. It will be seen that this allows for a careful examination of how the chemistry of the CMC system, specifically the hybrid energy states arising out of mixtures of cluster and molecule orbitals, affects transport. The second model for the leads considers them to be multimode or multichannel. The multichannel lead is constructed by periodically repeating a multi-atom unit cell in 1D. This is a more realistic model of nanocontacts which in reality have many different electron modes propagating at a given energy.

The strength of the coupling between the molecule and the clusters is a significant factor in the control of electron transport through the wires. For single-channel ideal leads, we find that for strongly coupled systems the highest occupied and lowest unoccupied molecular orbital (HOMO/LUMO), do not necessarily control the conduction of electrons. For this case transport is mediated by states that are mixtures of those in the clusters and the molecule. In our calculations with multimode leads, the same is true, and also the molecule is found to be very conductive (more so than has been reported experimentally[9]). By increasing the bond lengths between the sulfur and the gold clusters, thereby

weakening the coupling, it is found that the magnitude of the transmission decreases and that the resonances in the transmission can be related to energy levels of the isolated molecule. However, to reduce the transmission to experimental levels the bond lengths have to be stretched to unphysical dimensions.

In Sec. II, we describe the scattering and transport theory used in this work. It is a method for solving the tight-binding form of the Schrödinger equation for the t matrix and transmission coefficients. The electronic structure of isolated BDT is discussed in Sec. III. To explore the effects of coupling in the simplest possible context, the results of a transmission calculation for BDT connected directly to ideal single-channel leads are described in Sec. IV. The evolution of the energy eigenstates of the system when Au clusters are attached to the BDT is discussed in Sec. V. The calculated transmission and conductance for various BDT-cluster systems attached to one-mode leads is presented in Sec. VI. Sec. VII describes the calculated transmission and conductance for multimode leads. Our conclusions are presented in Sec. VIII.

II. TRANSPORT THEORY

A. Landauer formula

We consider the transport of electrons through a molecular system by modeling it as a one-electron elastic scattering problem. The molecule acts as a defect between two metallic reservoirs of electrons. An electron incident from the source lead with an energy E, has a transmission probability $T(E)$ to scatter into the drain lead. By determining the transmission probability for a range of energies around the Fermi energy, ϵ_F of the lead, the finite temperature, finite voltage, Landauer formula can be used to calculate the transmitted current I as a function of the bias voltage, V, applied between the source (left lead) and drain (right lead):

$$I(V) = \frac{2e}{h} \int_{-\infty}^{\infty} dE\, T(E) \left(\frac{1}{\exp[(E-\mu_s)/kT]+1} - \frac{1}{\exp[(E-\mu_d)/kT]+1} \right).$$
(1)

The two electrochemical potentials μ_s and μ_d, refer to the source and drain, respectively. They are defined to be, $\mu_s = \epsilon_F + eV/2$ and $\mu_d = \epsilon_F - eV/2$. The differential conductance is then given by the derivative of the current with respect to voltage.

B. Evaluation of the transmission matrix

We find the multichannel transmission probability $T(E)$ by solving the Schroedinger equation directly for the scattered wave functions. This is done by setting up a set of equations involving the transmission and reflection matrices for the modes of the leads that are coupled to the molecule. We treat the Hamiltonian using the tight-binding approximation in a nonorthogonal atomic basis set. The formalism we use differs from other tight-binding methods involving Green's-function techniques[10] and transfer-matrix methods.[19] For the one-electron tight-binding Hamiltonians used it yields exact results.
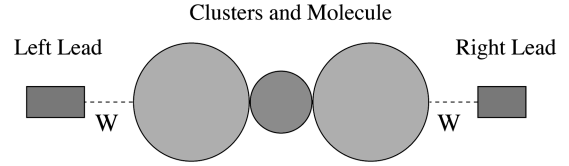

FIG. 1. Schematic diagram of the three noninteracting systems: left lead, CMC, and right lead. The systems are coupled by the potential W.

We start with Schrödinger's equation, $H|\Psi^\alpha\rangle = E|\Psi^\alpha\rangle$, where $H = H_0 + W$ is the Hamiltonian for the entire coupled system composed of the left lead, clusters + molecule (CMC) and right lead. The Hamiltonian H_0 is that for the decoupled system consisting of isolated left and right leads and the CMC. The ideal leads are then coupled to the CMC system via the coupling potential W. A schematic of the model system is shown in Fig. 1. The wave function $|\Psi^\alpha\rangle$, which describes an electron with energy E, propagating initially in the αth mode of the left lead, will be written using LCAO in a nonorthogonal set $\{|n,j\rangle\}$. Here n labels the site (or unit cell) and j labels the atomic orbital on the site. $|\Psi^\alpha\rangle$ is expressed in terms of the transmission and reflection matrices, $t_{\alpha,\alpha'}$ and $r_{\alpha,\alpha'}$ and has different forms in the left lead (L), CMC (M), and right lead (R). The total wave function is a sum of these three, $|\Psi^\alpha\rangle = |\Psi_L^\alpha\rangle + |\Psi_M^\alpha\rangle + |\Psi_R^\alpha\rangle$, where

$$|\Psi_L^\alpha\rangle = \sum_{n=-\infty}^{n=-1} \sum_j \left(c_j^\alpha e^{iny^\alpha} + \sum_{\alpha' \in L} r_{\alpha',\alpha} c_j^{\alpha'} e^{iny^{\alpha'}} \right) |n,j\rangle,$$
(2)

$$|\Psi_M^\alpha\rangle = \sum_j a_j^\alpha |0,j\rangle,$$
(3)

$$|\Psi_R^\alpha\rangle = \sum_{n=1}^{n=\infty} \sum_j \sum_{\alpha' \in R} t_{\alpha,\alpha'} d_j^{\alpha'} e^{iny^{\alpha'}} |n,j\rangle.$$
(4)

The forms for the wave function in the left and right leads can be interpreted in the following way. $|\Psi_L^\alpha\rangle$ is composed of a rightward propagating Bloch wave along with reflected leftward propagating and decaying evanescent modes in the left lead. For the right lead, $|\Psi_R^\alpha\rangle$ is a sum over the transmitted rightward propagating and decaying evanescent modes in the right lead. All modes in both leads have energy E. Note that in the leads the site index n labels the unit cells of the leads and the sum over j is over all orbitals in a multi-atom unit cell. The CMC is assigned the site label $n=0$ and there j runs over all of the atomic orbitals of the CMC. The Bloch coefficients, c^α and d^α, for the left and right leads, respectively, and the reduced wavenumbers y^α are calculated for the various modes using a transfer-matrix method outlined in the Appendix.

Using Schrödinger's equation and applying the bra $\langle n,i|$, the following system of linear equations is arrived at for the unknown quantities, $r_{\alpha',\alpha}$, a_j, and $t_{\alpha',\alpha}$:

$$\sum_{\alpha' \epsilon L} r_{\alpha',\alpha} \sum_{m=-\infty,j}^{m=-1} A_{n,m}^{i,j} c_j^{\alpha'} e^{imy^{\alpha'}} + \sum_j A_{n,0}^{i,j} a_j^{\alpha}$$

$$+ \sum_{\alpha' \epsilon R} t_{\alpha',\alpha} \sum_{m=1,j}^{m=\infty} A_{n,m}^{i,j} d_j^{\alpha'} e^{imy^{\alpha'}}$$

$$= - \sum_{m=-\infty,j}^{m=-1} A_{n,m}^{i,j} c_j^{\alpha} e^{imy^{\alpha}}, \tag{5}$$

where $A_{n,m}^{i,j} = H_{n,m}^{i,j} - ES_{n,m}^{i,j}$ with the Hamiltonian matrix, $H_{n,m}^{i,j} = \langle n,i|H|m,j \rangle$ and the overlap matrix, $S_{n,m}^{i,j} = \langle n,i|m,j \rangle$, being introduced explicitly. The overlap matrix is defined as the overlap between orbitals i and j on sites n and m, respectively. This incorporates the nonorthogonal basis set into the theory. The Hamiltonian matrix consists of a sum of the free Hamiltonian matrix, $(H_0)_{n,m}^{i,j}$, and the coupling matrix, $W_{n,m}^{i,j}$.

We now proceed to define the relevant matrices for our model. As with the wave functions, the free Hamiltonian, H_0, is partitioned into the three systems, (L), (R) and (M). We assume that the atomic orbitals on each lead are mutually orthogonal and only hopping between nearest-neighbor cells is considered. Thus the Hamiltonian matrix for the leads is composed of a matrix ϵ consisting of (atomic) site and intracell hopping energies and a matrix β of all the intercell hopping energies between atoms of nearest-neighbor cells. The Hamiltonian elements for the CMC are taken to be extended Hückel matrix elements between all orbitals on the CMC. The extended Hückel method is an empirical LCAO quantum chemistry method that provides a reasonable approximation to energies for molecular systems such as those being studied in this paper. More sophisticated *ab initio* quantum chemistry methods can also be used to evaluated these matrix elements.

We also use extended Hückel to estimate the interaction between the leads and the CMC. The coupling matrix, W, is taken to consist of the Hückel matrix elements between all of the orbitals in the unit cells directly adjacent to the CMC and all orbitals of the CMC. All other matrix elements are assumed to be zero.

Some assumptions are also made about the overlap matrix $S_{n,m}^{i,j}$. As was mentioned above, the orbitals on the leads are assumed to be orthogonal to one another. Also, the overlap between orbitals on the lead and orbitals on the CMC will be assumed zero. However, the orbitals on the CMC will not be assumed to be orthogonal to each other.

With the matrices that enter Eq. (5) thus defined, we solve Eq. (5) numerically for the reflection and transmission coefficients $r_{\alpha',\alpha}$ and $t_{\alpha',\alpha}$ for each rightward propagating mode α at energy E in the left lead. The total transmission and reflection are then given by

$$T(E) = \sum_{\alpha \epsilon L} \sum_{\alpha' \epsilon R} \frac{v^{\alpha'}}{v^{\alpha}} |t_{\alpha',\alpha}|^2, \tag{6}$$

$$R(E) = \sum_{\alpha \epsilon L} \sum_{\alpha' \epsilon L} \frac{v^{\alpha'}}{v^{\alpha}} |r_{\alpha',\alpha}|^2, \tag{7}$$
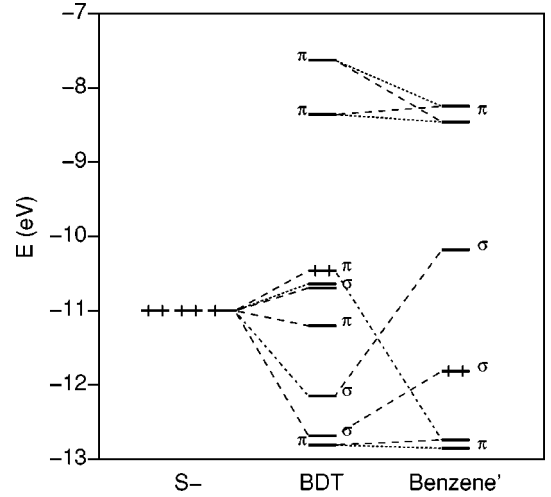

FIG. 2. Energy level diagram for BDT ion. Left diagram shows the p orbitals for one of the sulfur ions (S) (not shown is the sulfur S level, which is lower in energy). Right diagram is for benzene with the 1,4 H's removed. The dashed lines connecting the diagrams indicate where the levels of a given segment get mixed into the BDT ion. The HOMO's are identified as the levels with the vertical line segments crossing the energy level.

where v^{α} is the velocity of the electron in the αth rightward propagating mode in the left lead. The sum over α' in the expression for T is over the rightward propagating modes at energy E in the right lead. For R the sum over α' is over the leftward propagating modes in the left lead.

III. ELECTRONIC STRUCTURE OF BDT

The molecule studied in this paper is 1,4 benzene-dithiolate (BDT). The ring of π conjugated carbon atoms provides delocalized electrons beneficial for conduction. The sulfur atoms on either end of the molecule bind to the two metallic leads. The nature and effects of this binding will be explored in the sections to follow. However, before examining the coupled system it is important to consider the electronic structure of the isolated molecule.

In Fig. 2 the electronic structure of BDT is shown in the middle diagram. The energy levels were calculated using extended Hückel. The geometry of the molecule was taken to be that of benzene with the 1,4 hydrogens replaced with sulfur. The sulfur-carbon bond was taken to be 1.795 Å. It should be noted that the molecule is technically an ion since the sulfurs each have an extra electron, given up by the hydrogens in changing from a thiol to a thiolate. The BDT is similar to simple benzene in that its HOMO and LUMO are both π-like orbitals. To the right of BDT in the figure are the energy levels for benzene with the H's at positions 1 and 4 removed (labeled Benzene'). The HOMO-LUMO gap for BDT is smaller than that of benzene. For benzene (not benzene') the HOMO is at -12.814 eV with a LUMO of -8.248 eV. It is shown in the diagram where the benzene' levels mix into the BDT. For BDT the HOMO is at -10.470 eV and the LUMO is at -8.247 eV. The character of the BDT HOMO is that of C π on the ring with some S π content. The other levels in the BDT spectrum, as marked on the diagram, also contain C π and C σ bonding states. The σ states are due to the two states in the benzene' spectrum that
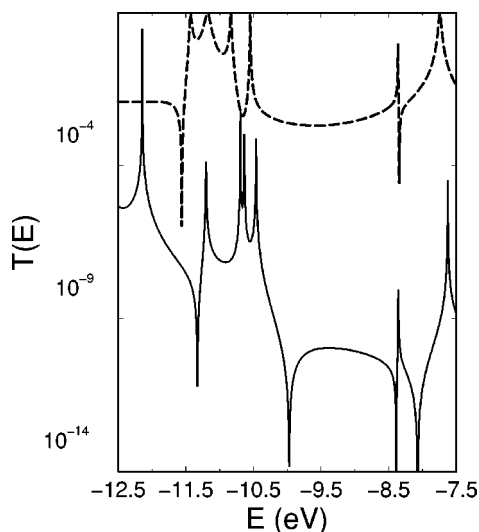
FIG. 3. Transmission diagrams for BDT connected directly to two ideal leads. The solid line corresponds to weak coupling, while the dashed line is for strong coupling to the molecule.

occur within the HOMO-LUMO gap of benzene. The figure also shows where the $2p$ orbitals of the sulfur (on the left in the diagram) mix into the molecular orbitals. The levels around the BDT HOMO contain significant S content, while the levels around the LUMO have less S character. The levels that have S character will be influenced strongly when the molecule is bonded to the gold clusters.

IV. TRANSMISSION IN A SIMPLE COUPLED BDT SYSTEM

We now proceed to apply the transport theory described in Sec. II by considering to start with a very simple model system: a CMC consisting only of a BDT molecule bonded directly to ideal 1D leads. The unit cell of the leads has one gold atom with only $6s$ orbitals. Thus there is only one energy band and only a single mode for the incident electrons. This allows us to explore the transmission in the simplest possible environment. We use the Hückel matrix elements between the orbitals on the two gold atoms adjacent to the molecule and all orbitals on the molecule as the matrix elements of **W**. Two cases of coupling will be studied.

The first case is of weak coupling. This means that the leads are not well-bonded to the molecule with a lead to sulfur distance greater than 4 Å. Because of the weak interaction between the leads and the molecule one would expect the molecular levels not to be significantly altered by the presence of the leads. This is indeed the case and is seen in Fig. 3. The solid curve, which represents the transmission through the molecule at weak coupling, has resonances (transmission maxima) at energies close to the molecular levels of isolated BDT. The relative strengths of the different resonances shown appear to be reasonable since from the energy level diagram of BDT the levels around the HOMO should be more conductive, due to having more S character. With less S content, the levels around the LUMO are less conductive.

The second case that we consider is typical of more realistic bonding distances of less than 3 Å. In this case the interaction between the lead and the molecule is not weak and one would expect the molecular levels to be influenced by the presence of the leads. The dashed line in the transmission plot is for this case. The resonances have shifted and broadened; some have disappeared. The nature of the levels has also changed, for example, the resonance at around -8 eV is now due to a σ level rather than a π LUMO level. This is a first example of the effects of mixing and much more will be made of this below.

Another interesting phenomenon is the occurrence of antiresonances where there is almost perfect reflection of the incident electron from the molecule. This arises from interference between the different molecular energy levels and from dynamics associated with the nonorthogonality of orbitals on different sites.[20,21] It will also be seen to occur in the results to follow.

The purpose of the above calculations was to show how even for a simple model the coupling between the molecule and leads plays an important role. For weak coupling, the molecular resonances survive and the transmission is identifiable with the molecular energy level structure. However, for strong coupling the electronic structure is modified significantly, which leads to resonances which depart from those of the isolated molecule and are often not related to the isolated molecular levels in any simple way. Clearly the chemistry needs to be considered carefully in studying transport in the more realistic models to be discussed next.

V. CMC MODELS: DIFFERENT BINDING SCHEMES

We now proceed to analyze the electronic structure and relevant chemistry for some models of CMC systems which we believe may represent the atomic structure of the contact region. It has been shown experimentally[22] that when 1,4 benzene-dithiol reacts with gold, it loses a pair of H ions to become BDT. The H ions react with the gold by capturing a valence electron and the sulfur bonds to the gold. No studies have as yet been done to characterize the nature of the interface between the sulfur and the gold nanowire. Recent studies of gold nanowires and break junctions of macroscopic gold wires have shown them to be different from bulk gold; the region between two gold contacts in a break junction is composed of filament structures.[23,24] The reconstructions of the Au atoms for a nanobridge tend to form hcp structures. Although it is not known whether either of the systems described in these reports is characteristic of the exact nature of the sulfur-gold interface, it seems reasonable to model the leads with different geometrical configurations that are consistent with the above findings for nanoscale gold structures.

Another area of uncertainty is the nature of the bond between the sulfur and the gold. An SCF calculation by Sellers *et al.*[25] has yielded calculated bond lengths and angles for alkanethiolate bonded over gold (100) and (111) surfaces. It is possible for the sulfur to bind over either a hollow site on the surface or directly over a gold atom. The binding over a hollow site has been calculated to be energetically favorable. Experiments on self-assembled monolayers (SAM's) tend to support the binding over hollow sites.[6] Recent theoretical studies have also shown that the hollow site is the favorable binding site for alkanethiol SAM's.[26] Similar calculations for BDT gold are not available at this time. Thus in the present
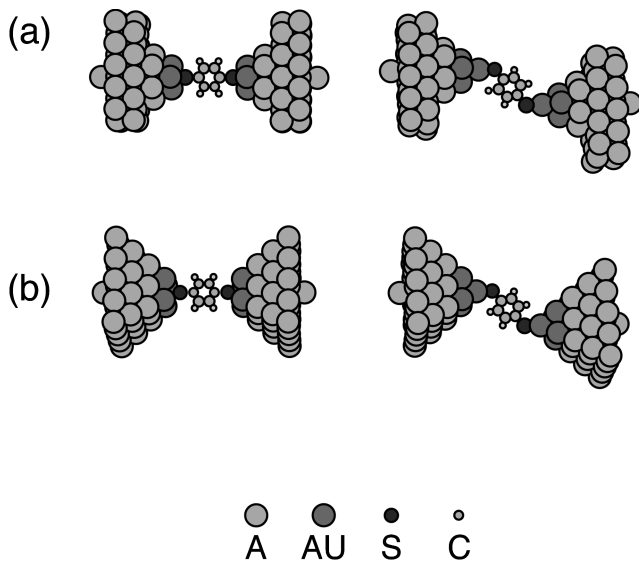
FIG. 4. Atomic diagrams of CMC systems. (a) (111) Au gold clusters with BDT. (b) (100) Au gold clusters with BDT. The left figures correspond to hollow-site binding, with the right figures showing on-site binding. The position of the single-mode leads is shown in the diagrams by the single gold atom attached to the outer faces of each of the gold clusters. For the multimode calculations, the outer two layers of each gold cluster form the unit cell used for the leads.
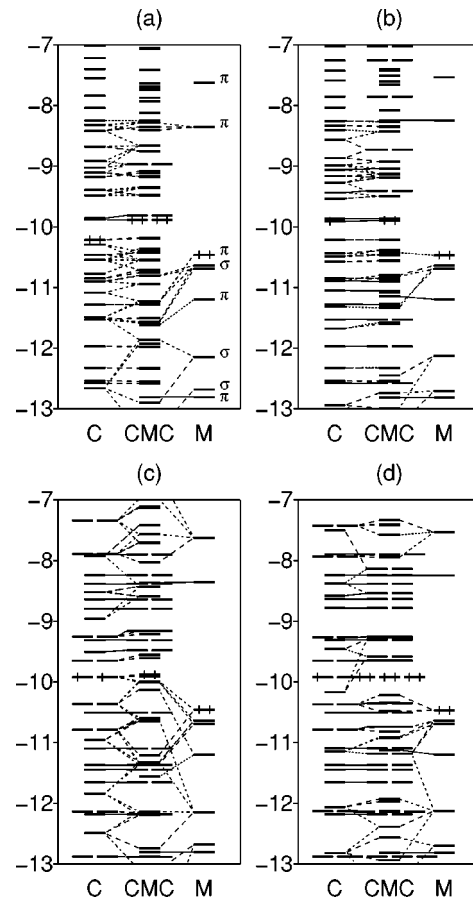

FIG. 5. Energy level diagrams for CMC systems. (a) (111) Au clusters with hollow-site binding. (b) (111) Au clusters with on-site binding. (c) (100) Au clusters with hollow-site binding. (d) (100) Au clusters with on-site binding. In the energy level diagrams, C labels the energy levels of the uncoupled left cluster, M labels the energy levels for the free molecule, and CMC labels the energy levels for the bonded clusters+molecule system. Energies are in eV.

work we study configurations in which the sulfur is bound over a gold atom as well as those in which it is bound over a hollow site. The lengths of the sulfur-gold bonds calculated by Sellers *et al.* are used in this paper.

The cluster contact geometries to be considered are shown in Fig. 4. In diagram (a), the gold clusters are arranged in an ideal fcc (111) configuration, where the lattice constant of bulk gold has been used to determine the spacing. The left CMC system is for hollow-site binding, where the S is bonded over a triangle of gold atoms. The perpendicular distance of the S over the triangle is 1.9 Å.[25] The right diagram of Fig. 4(a) is for binding directly over a gold atom. In this binding scheme the Au-S-C bond angle is not 180°. For alkanethiolate it was found to be around 110°,[25] but in order to match the experimental lead-lead distance of 8.5 Å for BDT,[9] we chose it here to be 130°. The bond length of the Au-S bond was taken to be 2.35 Å.[25] For the hollow-site binding there are 50 Au atoms in each cluster and 51 in each for the on-site binding.

The cluster geometry shown in Fig. 4(b) is for gold (100). Again the spacing has been determined using the lattice parameter of bulk gold. In the left figure the sulfur is bonded over a hollow site. In this case the hollow site is defined by a square of gold atoms. The perpendicular distance of the S over this square was taken to be 2.0 Å.[25] The right diagram is for the case of binding directly over a gold atom. Again the bond angle was assumed to be 130°, but the bond length was now assumed to be 2.15 Å.[25] The clusters for hollow-site binding have 54 Au atoms each and for on-site binding 55 Au atom clusters are used.

In the last CMC geometry studied we took the left cluster to be gold (100) and the right cluster to be (111). This was done to examine the effects of asymmetric binding, which may well occur since the two nanocontacts need not be iden-

tical. Both on-site binding and hollow-site binding configurations were considered. All the bond distances and angles were based on the previous geometries.

With these more realistic models of the contact region, the nature of the bonding of the clusters to the molecule is clarified by considering the electronic structure of the CMC. Extended Hückel was used to calculate the energy levels of the CMC. The ideal leads and most of the atoms in the gold cluster were modeled with just $6s$ orbitals. However, the gold atoms adjacent to the sulfur and responsible for most of the bonding to the sulfur were treated using the full valence orbital set. For gold, the electron Fermi level lies in the $6s$ band so that this treatment of the electronic structure makes it possible to study transport through fairly large clusters, while at the same time retaining a realistic description of the bonding between the BDT molecule and the gold.

The energy level diagrams for the various systems are shown in Fig. 5. To clarify the nature of the various levels the CMC was separated into three fragments: the left cluster (denoted by C in the figure), BDT (denoted by M), and the right cluster. It is shown in the diagram how the levels of these individual fragments get mixed into the overall electronic structure. In the binding geometries chosen above the

coupling of the molecule to the clusters is strong and the levels of the isolated BDT are strongly affected. It should be noted that in these calculations the first sites for the single-channel leads were also included in the calculation since, as was seen previously, the coupling **W** of the CMC to the ideal leads also influences the electronic structure. (In Fig. 4, the single gold atom bonded to the left and right gold clusters of each diagram indicates where this 1D gold chain was attached for the single-mode calculations.) For clusters of the size considered here this effect is not large, but for smaller clusters the effect can distort the electronic structure of the CMC very significantly.

Based on the four energy level schemes in the diagram it is possible to make some general statements. With the chosen sizes of the clusters the level structure of the cluster is quite dense. As the cluster size increases this level structure would eventually become the continuous energy bands of bulk gold. This is an attempt to take into account the continuum nature of the spectrum of the gold contacts in the model while still being able to address the chemical binding of the contacts to the molecule. It is also a useful way to estimate the Fermi level of the leads by using the HOMO of the cluster as an approximation. In all of the diagrams it is seen that the Fermi level of the clusters lies within the HOMO-LUMO gap of the BDT. It is also closer to the HOMO than to the LUMO. This has been suggested to be true[9,8] and the present calculations support this idea.

Another significant aspect of the diagrams is the strong mixing of the molecular states with cluster states. This mixing is significant in all diagrams. For the clusters in the (111) orientation, the molecular levels around the HOMO are predominantly shifted downwards, whereas for the (100) clusters the HOMO mixing is more symmetric in energy. The LUMO levels all tend to be mixed into the higher energy levels of the CMC system. The character of the levels also becomes mixed; it can be seen that some π levels of the molecule are mixed with σ states. In all the diagrams there is also a series of levels between -10 eV and -9 eV for which no molecular content is shown explicitly. However, these states contain complex, but small admixtures of many BDT levels. From these energy diagrams it appears the BDT HOMO-LUMO are not clearly identifiable in the energy level structure of the combined system for these cases which involve strong binding of the molecule to the clusters. Thus, transport in these systems will be very different from that through a free molecule.

The energy level diagrams for the asymmetric binding are not shown since they are qualitatively similar to those in Fig. 5, with the main difference being that degeneracies in the energy level spectrum are broken due to the lower symmetry of the system.

VI. TRANSMISSION AND CONDUCTANCE OF CMC SYSTEMS WITH SINGLE MODE LEADS

The electronic transmission through the above systems will now be calculated using leads with just a single propagating mode. By using leads with just one energy band we will be able to study the role of the chemistry in transport. We will use the single-electron channel to probe the energy level structure of the CMC systems. The leads are con-
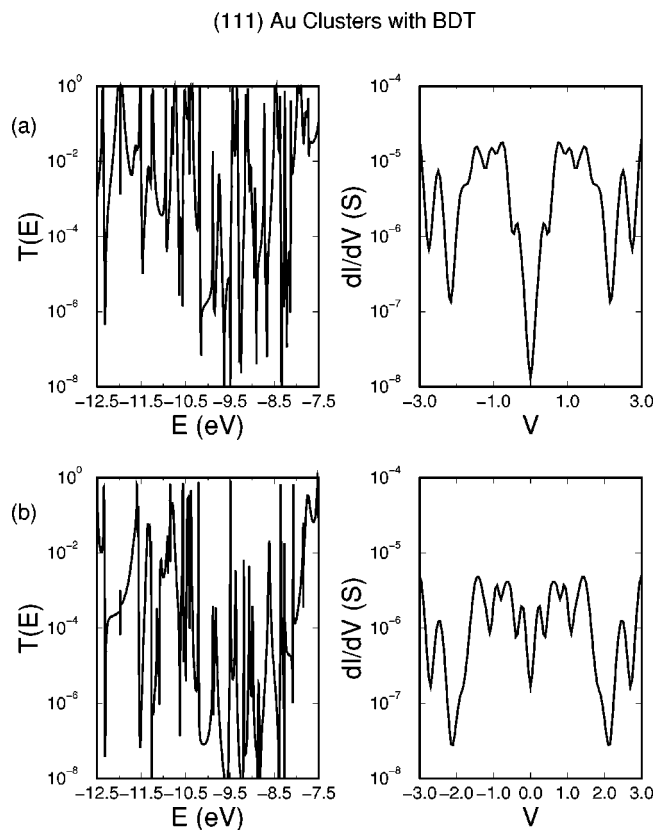

FIG. 6. Transmission and differential conductance for (111) Au clusters with BDT: (a) hollow-site binding; (b) on-site binding.

structed out of a unit cell containing one gold atom with a $6s$ orbital. The transmission probability $T(E)$ was calculated for energies around the Fermi level of the Au leads. The coupling matrix, **W**, was determined by evaluating the Hückel matrix elements between the ideal leads' $6s$ orbital on the sites adjacent to the CMC (shown as the single gold atoms attached to the outer faces of the gold clusters in Fig. 4) and all the orbitals of the CMC. The Landauer formula was then used to obtain the current vs bias voltage curve for each system. The differential conductance was calculated from this data.

In Fig. 6, the transmission and differential conductance diagrams are shown for the clusters in the (111) orientation. The top diagrams are for hollow-site binding and the bottom for on-site binding. There is significant transmission throughout most of the energy range with some overall reduction in the region from -10.5 eV to -9.5 eV. This corresponds to the levels in the energy diagram that have less molecular content. The transmission for on-site binding is on the whole of lesser magnitude than for the hollow-site case. This is because the molecule is less strongly bonded and the number of channels entering the molecule is less since it is only attached to one gold atom. The transmitting states are attributed to either delocalized π or σ bonding states of the molecule. For instance, in the transmission diagram of Fig. 6(a), the resonances between -12.5 eV and -11.5 eV are due to σ states, whereas the states around -10.5 eV to -11.5 eV are primarily π. The resonances between -8.5 eV and -8.0 eV are directly connected with the molecules LUMO as seen from the energy diagram, Fig. 5(a). The same can be said for the case of on-site binding. There, however,
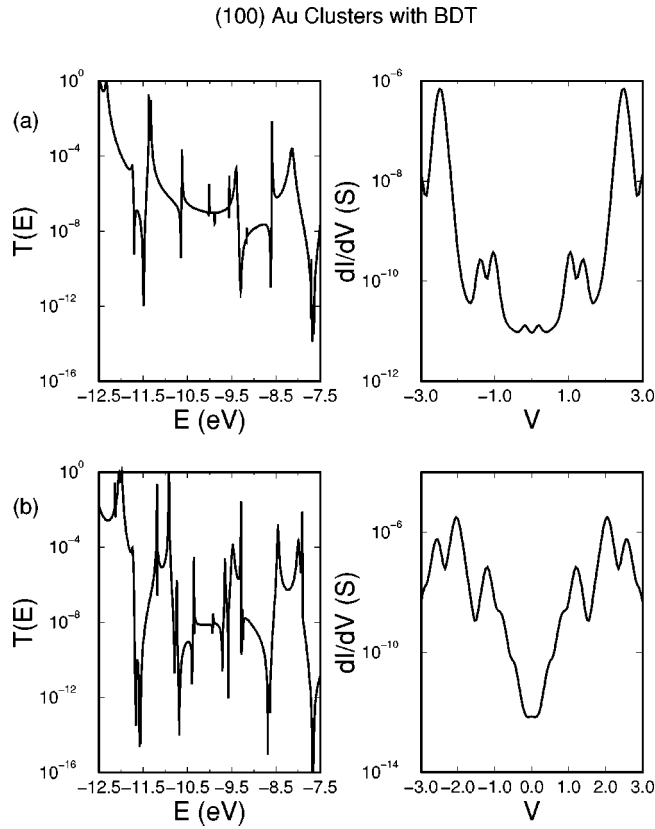
(100) Au Clusters with BDT

FIG. 7. Transmission and differential conductance for (100) Au clusters with BDT: (a) hollow-site binding; (b) on-site binding.

(111) and (100) Au Clusters with BDT

FIG. 8. Transmission and differential conductance for BDT bonded to (100) and (111) Au clusters: (a) hollow-site binding; (b) on-site binding.

the mixing is not as significant and the transport through states connected with the HOMO and LUMO is more noticeable. This is evidenced by the resonances at -10.5 eV where the states are from the HOMO. The states at -8.5 to -7.5 eV are from the two BDT states around the LUMO. In both cases the mixing of the molecule has led to the large transmission throughout the energy range.

The differential conductance curves for the two (111) clusters are shown also. The Fermi energy was arbitrarily chosen to be -10.1 eV for both of these calculations. Choosing a different Fermi energy can result in significantly different conductance characteristics for some calculations where the transmission has fewer resonances. However, in the present case, because of the many resonances that occur in the energy range of interest, the conductance is relatively flat and not very sensitive overall to the choice of Fermi energy. It is also significantly higher (by two orders of magnitude) than what was found experimentally.[9] This has also been found in other calculations on BDT.[27]

The transmission curves for the (100) oriented clusters presented in Fig. 7 have fewer resonances and the overall magnitude is lower. For this case the on-site transmission (b) has more resonances than the hollow-site case (a). This is because the sulfur is bonded more strongly to the single gold atom than over the four gold atoms. Again the molecular states are mixed with the cluster states. But it can be seen in the energy level diagrams, Figs. 5(c) and 5(d) that within the CMC spectrum there are levels that are almost entirely cluster levels. This is different than the (111) case where only a few of the CMC states were entirely cluster states. These states transmit very poorly. Those states that are more trans-
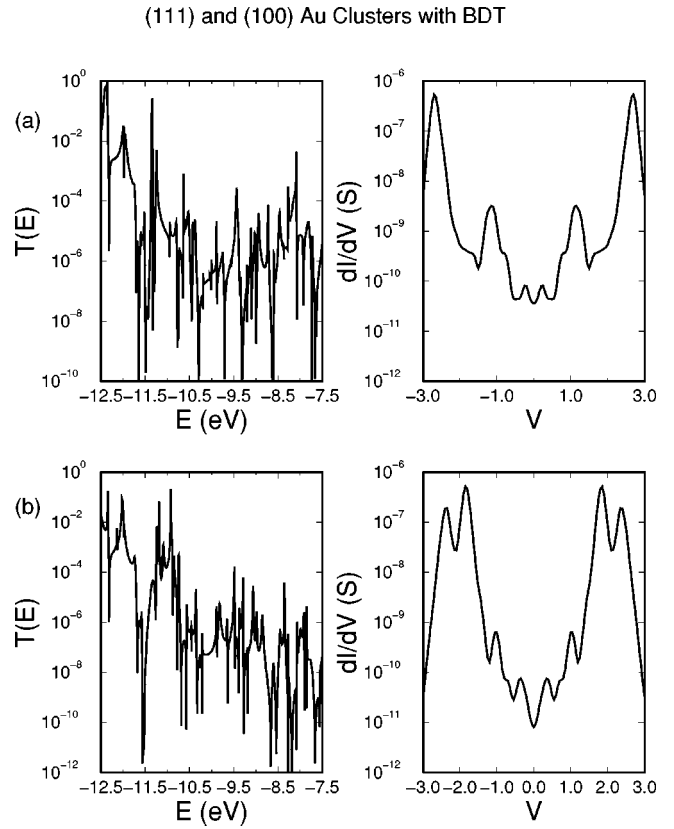
missive can again be identified as either delocalized σ or π states from the molecule. In both diagrams the resonances below -11 eV are due mostly to σ states, while the resonances around -9.5 eV to -10.5 eV are due to π states and again the resonances around -8.5 eV have BDT LUMO content. The lower magnitude in the transmission curves results in lower conductance compared to the previous results. For the differential conductance calculations the Fermi energy was arbitrarily chosen to be -10.0 eV.

Finally, in Fig. 8 we present results for the BDT molecule binding to two dissimilar clusters. In the calculated transmission curves, Figs. 8(a) and 8(b) the transmission now seems to share features of both the (111) and (100) oriented clusters. The magnitude of the transmission is lower than for the BDT connected to two (111) clusters (Fig. 6) and comparable to that for BDT connected to two (100) clusters (Fig. 7). The number of resonances present is similar to the pure (111) case. The differential conductance curves were calculated for a Fermi energy of -10 eV. Qualitatively, the structure of the curves agrees with the experimental findings[9] in that the differential conductance is very small at low bias and begins to increase strongly at bias voltages of the order of 1 V for this choice of Fermi energy. However, as for the cases of binding between identical clusters discussed above the differential conductance is again significantly larger than was reported experimentally.

VII. TRANSMISSION AND CONDUCTANCE OF CMC SYSTEMS WITH MULTIMODE LEADS

The previous section examined the transmission through CMC systems that had one-band ideal leads attached. This
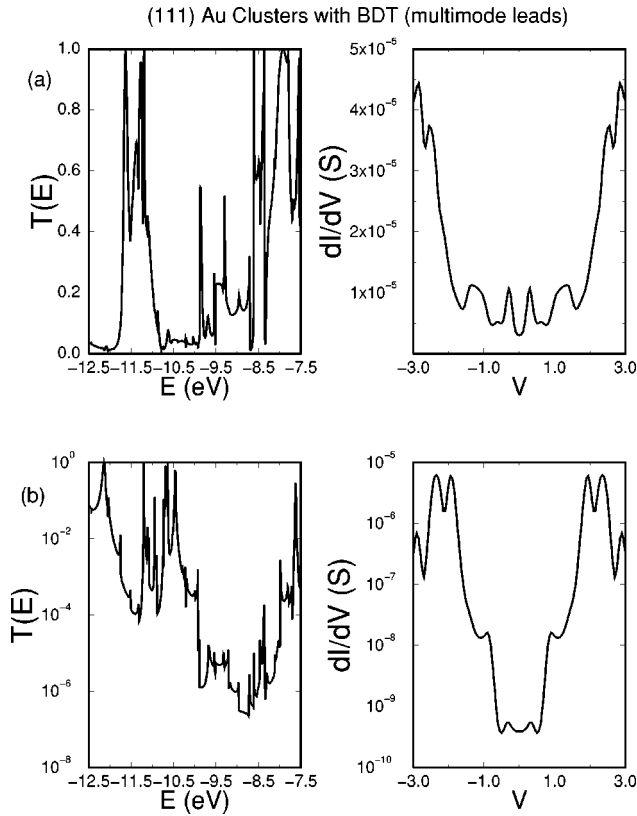
FIG. 9. Transmission and differential conductance for (111) Au multimode leads with hollow site binding to BDT: (a) is for strong bonding to the BDT, while (b) is for weak bonding.
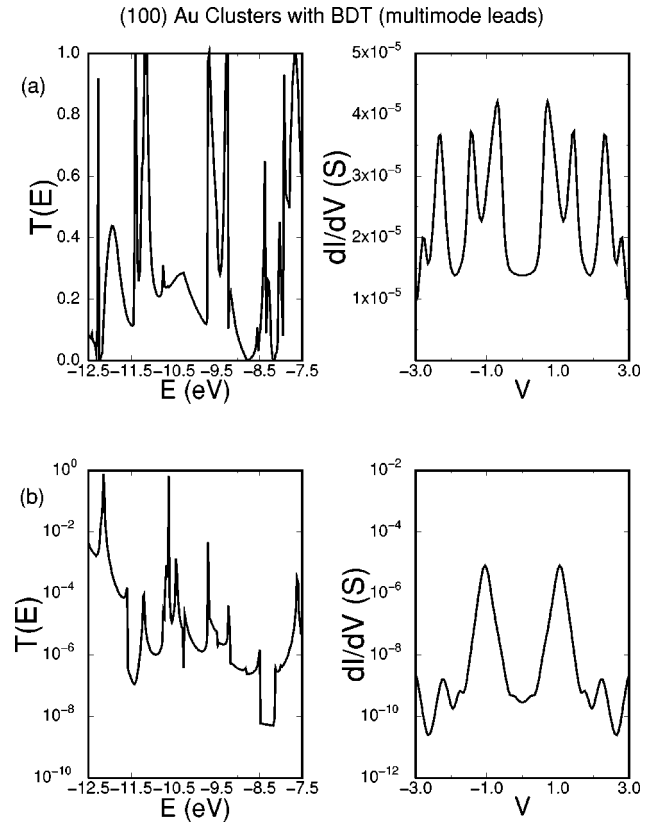

FIG. 10. Transmission and differential conductance for (100) Au multimode leads with hollow-site binding to BDT: (a) is for strong bonding to the BDT, while (b) is for weak bonding.

allowed the opportunity to relate resonances to the electronic structure of the contact area. We now attach multimode or multichannel leads to the CMC. The term multichannel lead is used to refer to leads that have more than one energy band. We construct such leads out of unit cells that contain more than one atomic orbital. By considering leads with unit cells containing more gold atoms we are able to model the many energy modes that exist within macroscopic gold contacts.

We again consider two different geometric configurations for the leads: (111) and (100) oriented gold contacts. For the lead in the (100) direction the unit cell is taken to consist of two layers of gold atoms. One layer has 16 atoms and the other has 25. Referring to the CMC diagrams previously shown, the unit cells for the (100) left and right leads are the outermost two layers of the gold clusters on the left and right in Figs. 4(a) and 4(b). For the (111) oriented lead the unit cell is again chosen to consist of two layers of gold atoms. It consists of two layers of 20 atoms each. To construct a lead with the structure of bulk gold in the (111) direction, actually requires a unit cell containing three layers, but two were chosen in this work to keep the number of modes similar between the two orientations. Again, the outermost two layers of the gold clusters on either side in Figs. 4(a) and 4(b) comprise the left and right unit cells that we use. These unit cells are periodically repeated in 1D to form the ideal leads now used for these multimode calculations. We use these unit cells with the gold atoms treated with just $6s$ orbitals to calculate the band structure of the 1D leads.

For these multimode calculations the interaction matrix, $\mathbf{W}$, is taken to be the Hückel matrix elements between all of the $6s$ orbitals in the unit cells directly adjacent to the now smaller CMC, and all orbitals on the CMC.

The first case that is considered is that of hollow-site binding for the (111) leads. The transmission diagram is shown in Fig. 9(a). The overall magnitude is up significantly compared to the ideal 1D lead calculation. The peaks are also broadened. There is strong transmission in the energy regions where the cluster states have mixed with the molecular states. This occurs most prominently around -11.5 eV, where there exist resonances that can be connected with the HOMO states of the molecule. The other region of significant transmission is at around -8 eV, which is due to CMC states connected with the LUMO of the BDT. The region in between has resonances that arise from those states that are complex admixtures of cluster with molecular levels. The differential conductance was calculated with a Fermi level chosen at -10 eV. It is seen that the conductance magnitude is now much greater than what it was for the ideal lead calculations. The molecule seems to be very conductive when attached strongly to the (111) oriented wide leads.

The same general statements can be made about the transmission through the molecule when attached to the leads oriented in the (100) direction, Fig. 10(a). Comparing the transmission diagrams between the ideal 1D lead calculation and wide lead calculation it is seen that the overall structure is consistent. However, as was the case above, the magnitude is significantly up as well as the peaks having broadened. This again leads to a conductance which is greater than that found for the ideal lead calculations. The Fermi energy was chosen again to be -10.0 eV.
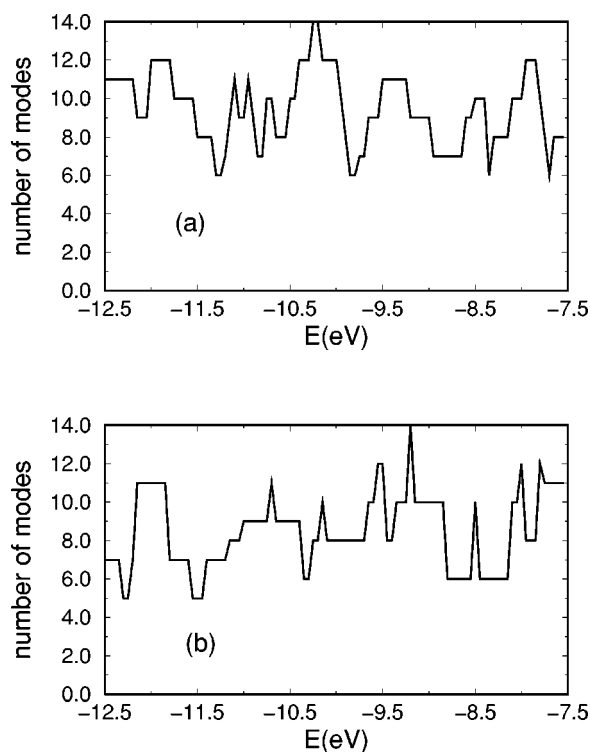
FIG. 11. Number of rightward propagating modes in $1d$ leads: (a) is for (111) Au leads, and (b) is for (100) Au leads.

The magnitude of the conductance found in the above two calculations exceeds that found experimentally. How far do the leads need to be separated from the molecule in this model to achieve experimental conductance magnitudes? This question is addressed by calculating the transmission for a system consisting of (111) or (100) oriented wide leads and the molecule with the perpendicular distance between the gold lead and the sulfur atom being 3.5 Å.

The transmission and conductance diagrams for these weak bonding cases are shown in Fig. 9(b) and Fig. 10(b), respectively. It can be seen that the transmission has gone down significantly in the region between -10.5 and -8 eV. For both cases, there are also now strong resonances that correspond almost exactly with the isolated molecular levels. (This is what we found previously for a weakly coupled system.) The other peaks in the spectrum, especially those in the region between -10.5 and -8 eV, can be directly attributed to the number of modes propagating in the lead. In Fig. 11, the number of modes propagating in the leads as a function of energy is shown. At these energies the tunneling transmission will be proportional to the number of modes in the lead. For the (111) leads, the transmission falls off sharply at -10.0 eV, corresponding to the drop in the number of modes. It then has peaks at around -9.5 and -8.5 eV, where the number of modes increases. Similar comments can be made about the transmission for the (100) leads. The weaker coupling of the molecule to the contacts has lowered the transmission and the conductance. Because there are order of magnitude fluctuations in $T(E)$ the conductance is now quite sensitive to the selection of Fermi energy. Different conductance curves can be obtained if the Fermi energy is chosen to occur on or off resonance. The same Fermi energies were used as in the strong bonding calculations. However, the calculated conductance is still somewhat larger than that reported experimentally, even for this case where in reality the molecule would probably not bond to the leads for the bond lengths considered.

VIII. CONCLUSIONS

In this paper we have presented a model which brings together techniques from chemistry and physics to analyze electron transport in molecular wires. The coupling of the molecule to the metallic contacts was studied by treating the contact region as a single chemical entity. By considering different cluster geometries and binding mechanisms we have been able to address two major unknowns in the experimental system: contact geometry and the S-Au bonding. We then proceeded to study the transport properties of these systems by attaching both single- and multimode ideal leads.

We presented three different transmission calculations. The first calculation was on BDT bonded directly to 1D ideal leads. This simple system showed how for weakly coupled systems the transmission is dominated by the energy levels of the free molecule. However, for strong coupling the energy levels of the free molecule are distorted and the transmission reflects this. The second set of calculations, which involved the attachment of different gold clusters to the BDT, explored the role of CMC chemistry by using single-mode ideal leads. The last calculation involved attaching multimode ideal leads, which model more realistic metallic contacts.

The second set of calculations showed that the transmission is sensitive to the choice of both geometry and bond. In these strongly coupled systems we have seen that the BDT states get mixed with the cluster states. The molecular HOMO and LUMO are not as prominent in the overall CMC level structure. The resulting transmission through the strongly coupled system departs from that of the isolated molecule. It was also found that cluster geometries which allow more cluster states to interact with the molecule, lead to greater transmission. This can be said of the (111) clusters compared to the (100) clusters. Lastly, the effect of lead asymmetry was to reduce the overall transmission and conductance relative to the purely (111) case.

The multimode lead calculations have shown that for the present class of models based on one-electron tight-binding theory and the standard extended Hückel parameters of quantum chemistry, the BDT molecule is quite conductive for reasonable bonding distances. Although the calculated differential conductance displays a gap of the order of 1 V at low bias in qualitative agreement with experiment, it was necessary to make the bond length between the molecule and the gold leads unphysically large in order to reduce the overall transmission magnitude to the experimentally observed range. The reason for this quantitative discrepancy between the theory and experiment is not known at present.

While transport through molecular wires has been discussed theoretically for some time, experiments on conduction through a single molecule chemically bonded between metallic contacts have only just begun to be performed and to provide a testing ground for theories. Clearly much remains to be learned both experimentally and theoretically about the mechanisms of electronic transport through these devices.

ACKNOWLEDGMENTS

APPENDIX

The modes for the wide leads were calculated using standard transfer-matrix theory. This method yields all the reduced wave numbers, y^{α}, and the Bloch coefficients c_j^{α}, for all the modes with energy E in a lead.

The transfer matrix considered here connects a Bloch state, $|\Psi\rangle = \Sigma c_j e^{iny}|n,j\rangle = \Sigma \Psi_{n,j}|n,j\rangle$, between nearest-neighbor sites. This can be written as

$$(\mathbf{T}(E))\begin{pmatrix} \mathbf{\Psi_n} \\ \mathbf{\Psi_{n-1}} \end{pmatrix} = \begin{pmatrix} \mathbf{\Psi_{n+1}} \\ \mathbf{\Psi_n} \end{pmatrix}. \tag{A1}$$

For a 1D chain treated in the tight-binding approximation, each unit cell will have a matrix ϵ containing the site energies and intracell hopping energies and a matrix β containing the intercell hopping energies. The transfer matrix for such a chain is

$$\begin{pmatrix} \beta^{-1} \cdot (E\mathbf{1} - \epsilon) & -\beta^{-1} \cdot \beta^{T} \\ \mathbf{1} & \mathbf{0} \end{pmatrix}. \tag{A2}$$

The eigenvalues and eigenvectors of this matrix provide the reduced wave numbers and Bloch coefficients, respectively.

---

*Electronic address: eemberly@sfu.ca

[1] A. Aviram and M. A. Ratner, Chem. Phys. Lett. **29**, 257 (1974).

[2] C. M. Fischer, M. Burghard, S. Roth, and K. von Klitzing, Surf. Sci. **361/362**, 905 (1995).

[3] C. Zhou, M. R. Deshpande, M. A. Reed, L. J. Il, and J. H. Tour, Appl. Phys. Lett. **71**, 611 (1997).

[4] R. P. Andres, J. D. Bielefeld, J. I. Henderson, D. B. Janes, V. R. Kolagunta, C. P. Kubiak, W. J. Mahoney, and R. G. Osifchin, Science **273**, 1690 (1996).

[5] C. A. Mirkin, R. L. Letsinger, R. C. Mucic, and J. J. Storhoff, Nature (London) **382**, 607 (1996).

[6] L. A. Bumm, J. J. Arnold, M. T. Cygan, T. D. Dunbar, T. P. Burgin, L. Jones II, D. L. Allara, J. M. Tour, and P. S. Weiss, Science **271**, 1705 (1996).

[7] B. C. Stipe, M. A. Rezaei, W. Ho, S. Gao, M. Persson, and B. I. Lundqvist, Phys. Rev. Lett. **78**, 4410 (1997).

[8] S. Datta, W. Tian, S. Hong, R. Reifenberger, J. I. Henderson, and C. P. Kubiak, Phys. Rev. Lett. **79**, 2530 (1997).

[9] M. A. Reed, C. Zhou, C. J. Muller, T. P. Burgin, and J. M. Tour, Science **278**, 252 (1997).

[10] M. P. Samanta, W. Tian, S. Datta, J. I. Henderson, and C. P. Kubiak, Phys. Rev. B **53**, R7626 (1996).

[11] M. Kemp, A. Roitberg, V. Mujica, T. Wanta, and M. A. Ratner, J. Phys. Chem. **100**, 8349 (1996).

[12] M. Magoga and C. Joachim, Phys. Rev. B **56**, 4722 (1997).

[13] S. Datta and W. Tian, Phys. Rev. B **55**, R1914 (1997).

[14] E. Emberly and G. Kirczenow, Ann. (N.Y.) Acad. Sci. **852**, 54 (1998).

[15] V. Mujica, M. Kemp, A. Roitberg, and M. Ratner, J. Chem. Phys. **104**, 7296 (1996).

[16] C. Joachim and J. F. Vinuesa, Europhys. Lett. **33**, 635 (1996).

[17] R. Landauer, IBM J. Res. Dev. **1**, 223 (1957); Phys. Lett. **85A**, 91 (1981).

[18] For a comprehensive review of Landauer theory and electron transport, see S. Datta, *Electronic Transport in Mesoscopic Systems* (Cambridge University Press, Cambridge, 1995).

[19] P. Sautet and C. Joachim, Phys. Rev. B **38**, 12 238 (1988).

[20] M. Kemp, A. Roitberg, V. Mujica, T. Wanta, and M. Ratner, J. Phys. Chem. **100**, 8349 (1996), and references therein.

[21] E. Emberly and G. Kirczenow (unpublished).

[22] P. E. Laibinis, G. M. Whitesides, D. L. Allara, Y. T. Tao, A. N. Parikh, and R. G. Nuzzo, J. Am. Chem. Soc. **113**, 7152 (1991).

[23] A. Correia and N. Garcia, Phys. Rev. B **55**, 6689 (1997).

[24] Y. Kondo and K. Takayanagi, Phys. Rev. Lett. **79**, 3455 (1997).

[25] H. Sellers, A. Ulman, Y. Schnidman, and J. E. Eilers, J. Am. Chem. Soc. **115**, 9389 (1993).

[26] K. M. Beardmore, J. D. Kress, N. Grønbech-Jensen, and A. R. Bishop, Chem. Phys. Lett. **286**, 40 (1998).

[27] M. Olson, Y. Mao, T. Windus, M. Kemp, M. Ratner, N. Eéon, and V. Mujica, J. Phys. Chem. **102**, 941 (1998).